



## Spring phenology and phenology-climate links inferred from two remotely sensed vegetation indices across regions and biomes

Xiyan Xu<sup>1</sup>, William J. Riley<sup>2</sup>, Charles D. Koven<sup>2</sup>, Gensuo Jia<sup>1\*</sup>

<sup>1</sup>Key Laboratory of Regional Climate-Environment for Temperate East Asia, Institute of Atmospheric Physics, Chinese Academy of Sciences, Beijing 100029, China

<sup>2</sup>Climate and Ecosystem Sciences Division, Lawrence Berkeley National Laboratory, Berkeley, California, USA

\*Corresponding Author:

Dr. Gensuo Jia

Key Laboratory of Regional Climate-Environment for Temperate East Asia,

Institute of Atmospheric Physics, Chinese Academy of Sciences,

Beijing 100029, China

Email address: [jjong@tea.ac.cn](mailto:jjong@tea.ac.cn)

Phone number: 86-10-82995314



1   **Abstract**

2           The timing of spring greenup (SG) as inferred by remotely sensed vegetation  
3   indices have showed contrasting dynamics across the same region and periods.  
4   Assessing the uncertainty in SG associated with different Normalized Difference  
5   Vegetation Index (NDVI) products is essential for robustly interpreting the links  
6   between climate and phenological dynamics. We compare SG inferred from two  
7   NDVI products over the period 2001-2013: (1) Terra Moderate Resolution Imaging  
8   Spectroradiometer (MODIS) and (2) National Oceanic and Atmospheric  
9   Administration's (NOAA's) Advanced Very High Resolution Radiometer (AVHRR)  
10   instruments processed by the Global Inventory Monitoring and Modeling Studies  
11   (GIMMS) to explore confidence and uncertainty in the NDVI-inferred SG trend and  
12   its links to climate variability. Both MODIS and GIMMS agreed in showing an  
13   advancement of SG in northern Canada, the eastern United States, and Russia, as well  
14   as a delay in SG in western North America, parts of Baltic Europe and East Asia. In  
15   the regions with advanced SG, GIMMS inferred much weaker advancement whereas  
16   in the regions with delayed SG, GIMMS inferred much stronger delay than MODIS.  
17   This resulted in a GIMMS SG delay in both North America and Eurasia. MODIS data  
18   show no significant SG shift in North American for spatial heterogeneity in SG shift,  
19   but dominant SG advancement in Eurasia. The SG advancement inferred from  
20   MODIS is associated with a stronger coupling between SG and temperature and a  
21   stronger sensitivity across biomes as compared to GIMMS. The main uncertainty in  
22   the SG trend and SG-temperature sensitivity are in northern high latitudes ( $>50^{\circ}\text{N}$ )  
23   where GIMMS and MODIS show different magnitude and sign of the annual SG  
24   anomalies. Compared to 1988-2000, inter-biome GIMMS SG-temperature sensitivity



25 is stable and the SG-temperature sensitivity increased in the boreal and Arctic biomes  
26 despite a slight reduction in the SG-temperature coupling over the period 2001-2013.  
27 The explanation for the increased SG-temperature sensitivity remains unclear and  
28 requires further investigation. We suggest broader evaluation of the NDVI products  
29 against field measurements and inter-validation for robust assessment of vegetation  
30 dynamics.

31 **Keywords:** NDVI, MODIS, GIMMS, phenology, spring greenup, sensitivity



## 1. Introduction

Vegetation phenology plays an important role in regulating land-atmosphere energy, water, and trace-gas exchanges. As the time spanned by satellite-based Normalized Difference Vegetation Index (NDVI) products has increased to longer periods, several studies have used NDVI to derive spring greenup time (SG) at regional and global scales. Several changes in SG have been documented in the past half-century in response to ongoing climate change. The Northern Hemisphere SG has advanced in the range of 0-12 days per decade as inferred by NDVI (Table 1). The wide range of SG shifts stem from studies covering different periods and regions, and different methods and datasets that have been applied to derive phenology metrics.

Many factors associated with the obtaining of satellite data—e. g. drift of satellite orbits, calibration uncertainties, inter-satellite sensor differences, bidirectional and atmospheric effects—may cause uncertainties in satellite derived data time series and thereby the uncertainties in interpreting the vegetation dynamics. Four NDVI products have been published based on radiances collected by the Advanced Very High Resolution Radiometer (AVHRR) instruments carried by programs of NOAA/NASA Pathfinder (PAL): Global Inventory Monitoring and Modeling Studies (GIMMS), Land Long Term Data Record (LTDR) version 3 (V3) and Fourier-Adjustment, Solar zenith angle corrected, Interpolated Reconstructed (FASIR). Each of these records extends back to the year 1981. Because of their long time span, the AVHRR NDVI products have been applied in numerous regional to global vegetation phenology studies (Table 1). Advantages are recognized for GIMMS NDVI over the other AVHRR NDVI products to represent the temporal variation of NDVI (Beck et al., 2011). The more recent NDVI products retrieved from Terra Moderate Resolution Imaging Spectroradiometer (MODIS) and Système Pour l’Observation de la Terre



(SPOT) VEGETATION mission (1 km)(e.g., Durpaire et al., 1995) are considered an improvement over AVHRR for improved calibration and atmospheric corrections, and higher spatial resolution (Zhang et al., 2003).

Several inter-comparisons have been conducted to evaluate the quality of different NDVI products. Yet broad validation of NDVI products by using field measurements is limited. The SPOT-4 VGT was used to evaluate the AVHRR PAL (1998-2000) and AVHRR GIMMS (1998-2004) NDVI time series for African continent. The dynamic range of SPOT-4 VGT NDVI is generally higher than the AVHRR PAL NDVI, but matched GIMMS NDVI, implying an improvement of GIMMS over PAL (Fensholt et al., 2006), however, the growing season GIMMS NDVI is lower than MODIS NDVI in African semi-arid environment (Fensholt and Sandholt, 2005). The annual average trend of GIMMS NDVI is consistent with MODIS NDVI in the semi-arid Sahel zone, but higher discrepancies in the more humid regions (Fensholt et al., 2009). In the north 50°N, four NDVI products (GIMMS3g, GIMMSg, SeaWiFS, SPOT) except MODIS showed consistent greening trend over overlapping period although differences in growing season NDVI and magnitude of greening trend pose uncertainties in satellite vegetation dynamics (Guay et al., 2014). In mixed grassland in the Grasslands National Park of Canada, both MODIS and AVHRR NDVI cannot quantify the spatial variation in ground based leaf area index measurements (Tong and He, 2013).

Despite inconsistencies and uncertainties among these NDVI products, GIMMS NDVI has been combined with other NDVI products to explore a longer period vegetation dynamics or to constrain potential data quality issue. Zhang et al. (2013) merged GIMMS NDVI over 1982-2000 with SPOT-VGT NDVI over 2001-2011 to investigate the SG in the Tibetan Plateau. GIMMS SG over 2001-2006 was



82 discarded for its delayed SG trend, in contrast to SPOT-VGT and MODIS SG trend,  
83 which was considered as a potential GIMMS NDVI data quality issue in the western  
84 Plateau. SG trend in Tibetan Plateau advanced by about  $10.4 \text{ days decade}^{-1}$  over 2001-  
85 2012 inferred from merged GIMMS and SPOT-VGT NDVI (Zhang et al., 2013), in  
86 contrast to the insignificant SG trend over 2000-2011 inferred from single GIMMS  
87 NDVI (Ding et al., 2016). The differences between GIMMS SG and SPOT-VGT and  
88 MODIS SG were also found after 2000s in western Arctic Russia where values and  
89 trends of MODIS and SPOT-VGT SG agreed very well (Zeng et al., 2013). When  
90 GIMMS NDVI was stitched with MODIS NDVI, the advancing trend of spring  
91 greenup in Northern Hemisphere over 2002-2012 that was inferred from MODIS  
92 NDVI is almost 3 times larger than the trend over the period 1982-2002 inferred using  
93 the GIMMS NDVI (Wang et al., 2016). However, a similar study using the GIMMS  
94 NDVI time series over 1982-2008 revealed an insignificant advancing trend in  
95 Northern Hemisphere over 2000-2008 in relative to 1980-1999 (Jeong et al., 2011).  
96 As the different methods in determining SG may not lead to such a high difference in  
97 SG trend (Cong et al., 2013), we hypothesize the different NDVI products may lead to  
98 the contradictory SG trend.

99 In this study, we attempt to better understand the causes of the differing findings  
100 of SG trend in previous studies. We compared SG as inferred by GIMMS and MODIS  
101 NDVI and their respective sensitivities to climate over the period 2000-2013, in  
102 which both the AVHRR and MODIS instruments were active. We used an  
103 independent climate reanalysis dataset to analyze the preseason, the period preceding  
104 SG during which the climate drivers regulate SG, and the sensitivity between  
105 preseason climate and SG. Data and methods are described in section 2. The results of  
106 comparison of GIMMS and MODIS SG, the preseason climate that regulates the SG



107 and sensitivities of the SG to pre-season climate are presented in section 3. Discussion  
108 and conclusions are given in section 4 and 5, respectively.

## 109 **2. Data and Method**

110

### 111 **2.1 Study area and biomes**

112 We restricted our analysis to north of 30°N, where temperate and boreal  
113 vegetation dominate, since that is the region where phenology is expected to be most  
114 strongly controlled by the annual cycle of temperature and moisture availability. In  
115 order to analyze the phenology and its response to climate across biomes, we used  
116 global mosaics of collection 6 MODIS data products (MCD12Q1) in the IGBP  
117 classification of land cover types with spatial resolution of 0.5° x 0.5° to mask the  
118 satellite-based SG results. The global mosaics of MCD12Q1 with geographic  
119 coordinates of latitude and longitude on the WGS 1984 coordinate reference system  
120 (EPSG: 4326) (Channan et al., 2014) were re-projected from standard MCD12Q1  
121 with 500m resolutions (Friedl et al., 2010). We used the IGBP land cover  
122 classification for 9 biomes in 2012 (Table 1): Evergreen Needleleaf Forest (ENF),  
123 Deciduous Needleleaf Forest (DNF), Deciduous Broadleaf forest (DBF), Mixed  
124 Forest (MF), Open Shrublands (OS), Woody Savannas (WS), Grassland (GL),  
125 Permanent Wetland (PW), and Cropland (CP). We distinguish the grassland to the  
126 north of 60°N (GLN), which is more likely to be tundra, from grassland in the  
127 temperate south (GLS) due to their expected differences in climate and controls on  
128 phenology.

129



## 130    **2.2 Climate reanalysis**

131            We calculated daily mean air temperature ( $T_m$ ) and cumulative precipitation  
132 ( $P_c$ ) from 6-hourly, half-degree resolution CRU-NCEP (Climate Research Unit-  
133 National Centers for Environmental Prediction) v6 reanalysis to identify the preseason  
134 climate associated with SG. The CRU-NCEP v6 dataset, recently extended to 2014, is  
135 a combination of CRU TS v3.2  $0.5^\circ \times 0.5^\circ$  monthly climatology and NCEP reanalysis  
136  $2.5^\circ \times 2.5^\circ$  with six hours time step available in near real time  
137 (<http://forge.ipsl.jussieu.fr/orchidee/wiki/Documentation/Forcings>).

## 138    **2.3 NDVI products**

139            We used the latest version NDVI time series (GIMMS NDVI3g) derived from  
140 the AVHRR instrument on board the NOAA satellite series. This dataset spans the  
141 period from July 1981 to December 2013 with spatial resolution of  $1/12^\circ$  and  
142 bimonthly temporal resolution (Pinzon and Tucker, 2014).

143            We also used the 16-day MODIS NDVI composites (MOD13C1, collection 6)  
144 at  $0.05^\circ$  spatial resolution, and further performed data quality control. We regridded  
145 both GIMMS and MODIS NDVI data to  $0.5^\circ \times 0.5^\circ$  resolution by taking the mean  
146 value in a  $0.5^\circ \times 0.5^\circ$  pixel to match the spatial resolution of the CRU-NCEP  
147 reanalysis. For GIMMS NDVI3g, the algorithm has improved snow-melt detection  
148 and the pixels recognized with snow or ice were filled with average seasonal profile  
149 or spline interpolation (Pinzon and Tucker, 2014). The pixels flagged with snow/ice  
150 were given the NDVI values with the values from the previous nearest period without  
151 snow influence. Even though, the filled values are very close to zero in the dormant  
152 season and the near-zero values are smoothed by the piecewise logistic method  
153 described in section 2.3. SGs were derived from GIMMS NDVI 2001-2013 to fit the



154 time period of MOD13C1.

## 155 **2.4 Determination of SG and preseason climate**

156 We determined the preseason duration following the method of Shen et al.  
 157 (2014), but with a different climate reanalysis product and method for calculating SG.  
 158 We restrict our analysis to north of 30°N, where temperate and boreal vegetation  
 159 dominate, since that is the region where phenology is expected to be most strongly  
 160 controlled by the annual cycle.

### 161 **Day SG and mean day of SG**

162 We first applied piecewise logistic method (Zhang et al., 2003) to fit and  
 163 smooth the temporal variation of vegetation index data (NDVI) to vegetation growth:

$$164 \quad y(t) = \frac{c}{1+e^{a+bt}} + d \quad (1)$$

165 where  $t$  is time in days,  $y(t)$  is the vegetation index at time  $t$ ,  $a$  and  $b$  are fitting  
 166 parameters,  $c+d$  is the maximum vegetation index value, and  $d$  is the initial  
 167 background vegetation index, usually the minimum vegetation index value preceding  
 168 the growing season.  $D_{SG}$  is identified as the Julian date at which the rate of change in  
 169 the vegetation growth ( $y(t)$ ) is maximum.  $D_{SG}$  is the maximum of the curvature and  
 170 derived as the second derivative of equation (1). The mean  $D_{SG}$  ( $\bar{D}_{SG}$ ) in each pixel is  
 171 averaged over the analysis years. For the pixels with multiple growth cycles in a year,  
 172 we applied this piecewise logistic method to the first cycle, so that  $D_{SG}$  is the Julian  
 173 date at which the second derivative of  $y(t)$  is maximum for the first time in a year.

### 174 **Preseason period and preseason climate**

175 We calculated the preseason period separately for temperature and  
 176 precipitation. To do this, we first calculated  $T_m$  and  $P_c$  during the respective preseason



177 periods. We defined the preseason climate ( $T_m$  and  $P_c$ ) in each pixel over the period  
 178 preceding  $\bar{D}_{SG}$  from 15 to 120 days with an increment of 3 days. We expect the  
 179 relative variation in precipitation to be more relevant than absolute values in  
 180 determining phenology, thus we used the relative variation of cumulative precipitation  
 181 in percentage (%) of precipitation change instead of the absolute cumulative  
 182 precipitation variation in millimeter (mm). We detrended the calculated  $T_m$  and  $P_c$   
 183 over the historical period. For each period preceding  $\bar{D}_{SG}$  for a given pixel, we  
 184 calculated the Pearson's correlation coefficients (PCC) between  $D_{SG}$  and  $T_m$  (and  $P_c$ ).  
 185 We screened the data to remove pixels where we found a positive interannual  
 186 correlation between (1) preseason temperature and  $D_{SG}$  and (2) preseason  
 187 precipitation and  $D_{SG}$ , respectively. We defined the period with the most negative  
 188 correlation between  $D_{SG}$  and  $T_m$  (and  $P_c$ ) as the preseason  $P_T$  (and  $P_P$ ). The length of  
 189 preseason (days) for temperature and precipitation control is defined as  $L_{PT}$  and  $L_{PP}$ ,  
 190 respectively. The superscript of  $G$  and  $M$  represents the variables derived from  
 191 GIMMS and MODIS, respectively (e.g.  $D_{SG}^M$  and  $L_{PT}^M$  are  $D_{SG}$  and  $L_{PT}$  derived from  
 192 MODIS, respectively.).

### 193 **SG response to preseason climate**

194 We calculated the response of SG to preseason climate by calculating linear  
 195 regressions between  $D_{SG}$  and  $T_m$  (and  $P_c$ ). We excluded the SG response to preseason  
 196 climate in pixels where no significant relationship was found (i.e.,  $p$ -value  $> 0.1$ ).

## 197 **3. Results**

### 198 **3.1 MODIS and GIMMS SG comparison**

199 The spatial pattern of GIMMS-inferred mean  $D_{SG}$  ( $\bar{D}_{SG}^G$ ) and MODIS-inferred  
 200  $D_{SG}$  ( $\bar{D}_{SG}^M$ ) is consistent ( $r = 0.83$ ,  $p < 0.01$ ). The regions with evident difference



201 between  $D_{SG}^G$  and  $D_{SG}^M$  are in the circumpolar Arctic and Asia high-altitudes (Figure 1a  
202 and 1b) where correlations between the time series of  $D_{SG}^G$  and  $D_{SG}^M$  are relatively low  
203 (Figure S1a). About 47% of the pixels in the north of 30°N have the inter-annual  
204 correlation above 0.5 ( $p < 0.1$ ), 86% of which are located between 45-90°N. The  
205 better correlated  $D_{SG}^G$  and  $D_{SG}^M$  time series to the north of 45°N than in lower latitudes  
206 implies agreed inter-annual variation of  $D_{SG}^G$  and  $D_{SG}^M$  in this region. In the regions  
207 with well-correlated inter-annual variation,  $D_{SG}$  differences between MODIS and  
208 GIMMS still show significant latitudinal characteristics (Figure S1b). In the northern  
209 mid-latitudes, we inferred a later  $\bar{D}_{SG}$  using MODIS ( $9 \pm 6$  days) in 67% of the pixels,  
210 and an earlier  $\bar{D}_{SG}$  ( $5 \pm 4$  days) in the remaining pixels, as compared to GIMMS. We  
211 also inferred a later  $\bar{D}_{SG}$  using MODIS in southern Asia and the eastern United States  
212 as compared to  $\bar{D}_{SG}$  using GIMMS. The  $D_{SG}^G$  and  $D_{SG}^M$  inter-annual variation are  
213 weakly correlated in the southern mid-latitudes, especially in the Eurasia. For those  
214 pixels in the south of mid-latitude, where inter-annual variation of  $D_{SG}^G$  and  $D_{SG}^M$  are  
215 well correlated,  $D_{SG}^M$  advanced  $D_{SG}^G$  by  $6 \pm 5$  days (Figure S1b).

216 Both MODIS and GIMMS agreed in showing that  $D_{SG}$  advanced in Northern  
217 Canada, Eastern United States, and Russia, and that  $D_{SG}$  delayed in western North  
218 America, parts of Baltic Europe and East Asia (Figure 1c and 1d). In the regions  
219 where  $D_{SG}$  advanced,  $D_{SG}^G$  advancement was much weaker than  $D_{SG}^M$ . In the regions  
220 where  $D_{SG}$  delayed, the  $D_{SG}^G$  delay is much stronger than  $D_{SG}^M$ . Together, these  
221 differences lead to a delayed continental-scale  $D_{SG}^G$  trend in both North America ( $0.80$   
222  $\text{days yr}^{-1}$ ) and Eurasia ( $0.22 \text{ days yr}^{-1}$ ) at 90% confidence level. MODIS implied no  
223 significant SG shift trend in North American but advanced SG trend of  $0.78 \text{ days yr}^{-1}$   
224 in Eurasia at 90% confidence level. The differences in  $D_{SG}^G$  and  $D_{SG}^M$  trend are mainly



225 in the northwest of North America and east-to-central Eurasia north of 50°N. The  
226 inter-annual variability of  $D_{SG}$  anomalies in relative to  $\bar{D}_{SG}$  over 2001-2013 indicated  
227 consistent anomaly signs of  $D_{SG}$  between MODIS and GIMMS over 30-50°N in North  
228 America. The most remarkable difference in  $D_{SG}$  anomaly between MODIS and  
229 GIMMS is in Northern North America (>50°N) where negative  $D_{SG}^G$  anomalies over  
230 2001-2008 and positive  $D_{SG}^G$  anomalies thereafter in North America, in opposite to  
231  $D_{SG}^M$  anomalies (Figure 2d). In Eurasia, both MODIS and GIMMS indicated anomalies  
232 of advanced  $D_{SG}$  in the north of 50°N after 2006 (Figure 2f). A large transition in the  
233  $D_{SG}^G$  anomaly occurred around 2000. The transition is particularly remarkable in North  
234 America, which is due to a 5-6 days later mean  $D_{SG}$  ( $\bar{D}_{SG}^G$ ) over 2001-2013 than that  
235 over 1982-2000 in North America.

### 236 3.2 Preseason climate regulating SG

237 The preseason length of temperature control for GIMMS ( $L_{PT}^G$ ) and MODIS  
238 ( $L_{PT}^M$ ) that we inferred from the correlation between  $T_m$  and  $D_{SG}$  differed due to the  
239 differences between  $D_{SG}^G$  and  $D_{SG}^M$  (Figure 3a, 3b). The spatial pattern of  $L_{PT}^G$  shows  
240 significant heterogeneity, with  $L_{PT}^G$  over two months in the regions from Russia to  
241 central Asia in Eurasia and from Alaska to northwestern Canada in North America.  
242  $L_{PT}^G$  is 62±38 days for all the valid pixels, while  $L_{PT}^M$  is usually less than two months,  
243 with the  $L_{PT}^M$  of 41±31 days. Moreover,  $L_{PT}^M$  is better correlated to  $T_m$  during its  
244 corresponding preseason ( $P_T^M$ ) with North Hemisphere correlation of 0.6±0.2 in  
245 comparison to the correlation between  $D_{SG}^G$  and  $T_m$  during its preseason ( $P_T^G$ ) of  
246 0.3±0.2 (Figure S2a, 2b).

247 The fraction of the northern mid- to high-latitude land surface with preseason  
248 precipitation control is less than that for temperature control for both GIMMS and



249 MODIS (Figure 3 and Figure S2). The pre-season length of precipitation control for  
250 MODIS ( $L_{pp}^M = 56 \pm 35$  days) is longer than that of temperature control. In contrast,  
251 GIMMS showed relatively shorter pre-season length of precipitation control ( $L_{pp}^G =$   
252  $45 \pm 32$  days) than that of temperature control. Although GIMMS showed a larger  
253 fraction of land surface where precipitation correlated to  $D_{SG}$  than MODIS, MODIS  
254 and GIMMS showed consistent spatial pattern in both pre-season length and  
255 correlations between  $P_c$  and  $D_{SG}$  (Figure S2c and S2d). The mean PCC is  $-0.4 \pm 0.2$  for  
256 both MODIS and GIMMS.

257 The spatial pattern of the temperature trend in  $P_T^M$  and  $P_T^G$  over 2001-2013 is  
258 consistent ( $r = 0.61$ ,  $p < 0.01$ ) although the derived pre-season length for temperature  
259 control differed for GIMMS and MODIS derived  $D_{SG}$  (Figure S3a and S3b). The  
260 majority of both North America and North Eurasia experienced warming of the SG  
261 pre-season, while Alaska, the eastern edge of Hudson Bay and the mid-latitudes of  
262 Eurasia ( $40-60^\circ\text{N}$ ) experienced a pre-season cooling. The pre-season warming trend is  
263 most significant in central Russia and eastern Canada and the cooling trend is most  
264 significant in part of Central Asia and central to eastern China. The maximum  
265 pre-season warming trend is about  $0.6^\circ\text{C yr}^{-1}$  in central Russia. The precipitation trend  
266 in the pre-season is insignificant and more heterogeneous as compared to the  
267 temperature trend for both  $P_P^M$  and  $P_P^G$  (Figure S3c and S3d). The spatial pattern of  
268 the precipitation trend in  $P_P^M$  and  $P_P^G$  are also less correlated ( $r = 0.40$ ,  $p < 0.01$ ) than  
269 that of temperature trend. Wetting of the pre-season occurred in mid to east of the  
270 United States, Western Canada, Northern Norway and Northwestern Russia. The  
271 largest value of the wetting trend is about  $7\text{ mm yr}^{-1}$ . Drying pre-season only occurred  
272 remarkably in the southeastern United States and scattered in Eurasia. The pixels  
273 where the largest values of a pre-season drying trend is about  $4\text{ mm yr}^{-1}$ .



### 274 3.3 SG sensitivity to preseason climate

275 The fraction of areas in which  $D_{SG}^M$  sensitive to  $T_m$  and  $P_c$  are much larger than  
276  $D_{SG}^G$  (Table S1) and  $D_{SG}^M$  are more sensitive to  $T_m$  and  $P_c$  in relative to  $D_{SG}^G$  (Figure 4).  
277 About 43% of the land fraction shows significant sensitivity of  $D_{SG}^M$  to  $T_m$  ( $p < 0.1$ )  
278 compared with 13% of the land fraction with significant sensitivity of  $D_{SG}^G$  to  $T_m$ .  
279 About 11% of the land fraction shows significant sensitivity of  $D_{SG}^M$  to  $P_c$  ( $p < 0.1$ ) as  
280 compared with 3% of the land fraction with significant sensitivity of  $D_{SG}^G$  to  $P_c$ . The  
281 sensitivity of  $D_{SG}^M$  to  $T_m$  is most significant in the mid- to high-latitudes (Figure 4b)  
282 whereas the sensitivity of  $D_{SG}^M$  to  $P_c$  is scattered (Figure 4d). The sensitivity of  
283 MODIS SG to precipitation is  $0.23 \pm 0.18$  days advancement per percent of  
284 precipitation increase. Due to the weak SG-precipitation coupling and sensitivity, we  
285 only analyzed biome-scale  $D_{SG}$  to  $T_m$  sensitivity (Figure 5). The difference between  
286 the sensitivity of  $D_{SG}$  to  $T_m$  as inferred by MODIS versus GIMMS is less in forest  
287 biomes, even though  $D_{SG}^M$  is more sensitive to  $T_m$  in all the biomes in relative to  $D_{SG}^G$ .  
288 The differences in  $D_{SG}$  to  $T_m$  sensitivity are especially significant in northern biomes.  
289 For example, sensitivity of  $D_{SG}^M$  to  $T_m$  in open shrublands, northern grasslands, and  
290 permanent wetlands are 50% higher than sensitivity of  $D_{SG}^G$  to  $T_m$  in these biomes.

291 As the GIMMS NDVI product extends as far back as the early 1980s, we also  
292 performed the comparison of  $D_{SG}^G$  to  $T_m$  sensitivity over two periods.  $D_{SG}^G$  to  $T_m$   
293 sensitivity was analyzed with the same method in section 2, but between the period  
294 spanning 1988 and 2000. This has the same length of time (13 years) as the later  
295 analysis period of 2001-2013. The fraction of area where  $D_{SG}^G$  shift in response to  $T_m$   
296 and  $P_c$  is reduced in the period 2001-2013 as compared to the earlier 1988-2000  
297 (Table S1). Most of the biomes show a slightly increased sensitivity of  $D_{SG}^G$  to  $T_m$  in  
298 the later period, as compared to that over 1988-2000, with the highest increase in the



299 northern grasslands (44.6%) and open shrublands (41.2%) (Figure 5a). The sensitivity  
300 of  $D_{SG}^G$  to  $T_m$  is relatively stable in southern grasslands. Exceptionally, the sensitivity  
301 of  $D_{SG}^G$  to  $T_m$  declined by 1.4 days  $^{\circ}\text{C}^{-1}$  for deciduous broadleaf forests and 0.1  
302 days  $^{\circ}\text{C}^{-1}$  for mixed forests; this represents a reduced sensitivity of 33.7% and 3.4%  
303 respectively. The inter-biome variation of the sensitivity of  $D_{SG}^G$  to  $T_m$  is stable ( $r =$   
304 0.90,  $p < 0.001$ ) over the two periods (Figure 5b).

## 305 4. Discussion

### 306 4.1 SG mean state and trend

307 We analyzed MODIS and GIMMS NDVI products to infer spring greenup dates  
308 and their responses to pre-season climate over the period 2000-2013. Inter-annual  
309 variation of greenup date as inferred from MODIS and GIMMS are well correlated  
310 north of 45°N (86% of the pixels with  $r > 0.5$  and  $p < 0.1$ ). But in these regions, we  
311 tend to infer a later greenup time using MODIS than GIMMS NDVI. This may be  
312 contributed by the evergreen vegetation and the influences of snow cover on the  
313 pixels. The snow cover led to NDVI gaps during the dormancy season. As a result, the  
314 time series of NDVI cannot be adequately fitted during the transitional snow melting  
315 and vegetation greening season (Zhou et al., 2015). We filled the snow-flagged  
316 MODIS NDVI with NDVI from previous period without snow contamination,  
317 whereas GIMMS NDVI was filled with average seasonal profile or spline  
318 interpolation (Pinzon and Tucker, 2014). Our MODIS filling potentially  
319 underestimate the NDVI during the transition season. In high latitudes with  
320 seasonal snowpack, the beginning of the growing season is often determined by  
321 snowmelt rather than temperature (Semenchuk et al., 2016). The study over  
322 Yamal Peninsula revealed that spring greenup date is almost the same as snow-end  
323 date between 70.0-73.5°N (Zeng and Jia, 2013), so that the snow cover affects the



324 identification of vegetation greenup. In the northern high latitudes at the selected  
325 locations in Canada and Sweden, even if the pixels influenced from snow cover are  
326 excluded, MODIS NDVI is lower than GIMMS NDVI in the dormant season  
327 (Fensholt and Proud, 2012). This can make an explanation to the late transition from  
328 dormant season to growing season by MODIS.

329 We inferred a heterogeneous trend in SG using both MODIS and GIMMS, but the  
330 sign and magnitude of the SG shift varies between MODIS and GIMMS. The main  
331 difference between the trend in SG as inferred by MODIS and GIMMS is in Alaska  
332 and Siberia, which lead to the main uncertainties in the NDVI derived SG trend in the  
333 northern high latitudes. The significant GIMMS SG delay in Alaska and mid-latitude  
334 Eurasia lead in general to a delay in SG in North America and Eurasia. In contrast, we  
335 inferred a delay in SG using MODIS in southern Alaska and eastern Canada offset SG  
336 advancement in eastern the United States and Canada, resulting in insignificant SG  
337 trend in North America. Significant SG advancement in Siberia resulted in strong SG  
338 advance in Eurasia. Even so, MODIS and GIMMS showed large inter-annual  
339 variability of SG anomalies in relative to the mean SG over 2001-2013 and the signs  
340 of the anomalies are consistent in between 30°N and 50°N. MODIS NDVI inferred  
341 mean SG advancement of 0.96 days year<sup>-1</sup> between 52-75°N over 2001-2013 at 90%  
342 confidence level in our results overwhelmed the MODIS snow-end date advancement  
343 of 0.37 days year<sup>-1</sup> in this region over 2001-2014 (Chen et al., 2015). The lagged  
344 snow phenology advancement implies that snow complication in determine SG in the  
345 cold regions is still present at a warmer climate.

#### 346 **4.2 SG dates sensitivities to climate**

347 The SG to preseason climate sensitivity by MODIS and GIMMS showed  
348 varied degree of vegetation-climate seasonal coupling. The higher correlation between



349 MODIS SG and preseason temperature indicates stronger MODIS SG-climate  
350 relationships. The stronger MODIS NDVI to temperature correlation than GIMMS  
351 NDVI was reported in central Europe, where the correlation between temperature and  
352 August NDVI anomalies were analyzed (Kern et al., 2016). The stronger SG-  
353 temperature coupling than precipitation is consistent with our previous study of SG to  
354 climate sensitivity over 1982-2005 (Xu et al., 2018). MODIS inferred stronger SG-  
355 temperature sensitivity in the northern boreal and Arctic biomes can be explained by  
356 the site-level observation that temperature sensitivity of phenology is greater in colder,  
357 higher latitude sites than in warmer regions (Prevéy et al., 2017). At the colder sites,  
358 the small changes in temperature may constitute greater relative changes in thermal  
359 budget (Oberbauer et al., 2013), so that the warming impacts on vegetation are  
360 amplified. This explanation is not applicable to the GIMMS NDVI inferred SG  
361 response to temperature that vegetation with earlier growing season is more sensitive  
362 to temperature (Shen et al., 2014).

363 The sensitivity of GIMMS SG to temperature increased over 2001-2013 in  
364 relative to that over 1988-2000. Our results showed SG to temperature sensitivity  
365 increased most significantly in Arctic grassland (44.6%), followed by other boreal  
366 biomes (open shrubland (41.2%), permanent wetland (35.9%), woody savanna (31.1%)  
367 and deciduous needleleaf forest (17.6%)). The magnitudes of enhanced sensitivity are  
368 even larger when we compare 2001-2013 SG-temperature sensitivity with a longer  
369 period over 1982-2005 (Xu et al., 2018). Compare with the period 1982-2005, SG-  
370 temperature sensitivity of the northern biomes (deciduous needleleaf forest, woody  
371 savanna, open shrublands and permanent wetlands) all increased more than 50% over  
372 2001-2013 with stable inter-biome sensitivity variation ( $r = 0.91, p < 0.01$ ).



373           The increased sensitivity of SG to temperature for boreal biomes has not been  
374 well investigated. In the contrary, temperature sensitivity of spring greenup may  
375 decline under warmer climate because (1) insufficient winter chilling may delay the  
376 spring greenup in spite of continued spring warming (Yu et al., 2010), (2) when  
377 spring greenup starts earlier, shorter photoperiod can limit the potential of leaf  
378 development (Chmielewski & Götze, 2016), (3) greenup may respond nonlinearly to  
379 temperature and be saturated at a high temperature (Caffarra & Donnelly, 2011), and  
380 (4) under warmer condition, the pre-season duration of thermal forcing can be reduced,  
381 which declines the SG-temperature sensitivity (Güsewell et al., 2017). The vegetation  
382 growth (represented by NDVI) to temperature sensitivity was reported declining in  
383 the growing season (April-October) based on GIMMS NDVI over 1982-2012 linked  
384 to water stress (Piao et al., 2014). In temperate ecosystems, the lower NDVI to  
385 temperature sensitivity coincidentally occurred with increased drought events. While in  
386 the arctic ecosystem, the lowered sensitivity of NDVI to temperature may be  
387 explained by increases in heat waves because the physiological response of  
388 photosynthesis to temperature is nonlinear with lower sensitivity under warmer  
389 conditions (Piao et al., 2014). The higher interannual temperature variability can also  
390 cause higher variations in water supply, thus the declined coupling between  
391 vegetation growth and interannual variability of growing season temperature,  
392 generally in semiarid regions (Wu et al., 2017). The wetting pre-season in mid to east  
393 of the United States, Western Canada, Northern land along Norway and Northwestern  
394 Russia may partly enhanced SG-temperature if the enhancement is validated.

### 395   **4.3 Uncertainties in SG as derived by MODIS and GIMMS NDVI**

396           With SG as inferred using GIMMS over the period 1988-2000 and as inferred  
397 using MODIS over 2001-2013, we found that the trend is advanced continuously in



398 response to a continuing trend in preseason warming. The uncertainties in the SG  
399 trend and its climatic sensitivity arise when SG as inferred using MODIS and GIMMS  
400 are compared together over the period 2001-2013. Wang et al.(2016) and Zhang et al.  
401 (2013) proposed that quality issues may present in GIMMS NDVI, which can bias  
402 vegetation growth sensitivity and growth trend. Instead of using continuous GIMMS  
403 SG over 1982-2011, Zhang et al. (2013) merged datasets of GIMMS SG over 1982-  
404 2000 and SPOT-VGT SG over 2001-2011 to detect SG trend due to data quality  
405 issues with GIMMS NDVI in most parts of western Tibetan Plateau, according to the  
406 findings of opposite GIMMS SG trend to SPOT-VGT and MODIS SG trend over the  
407 period 2001-2006. With this merged data record, the SG trend continuously advanced  
408 in Tibetan Plateau over 1982-2011. This result is consistent with the SG trend derived  
409 from tree-ring data (Yang et al., 2017). On the contrary, continuous GIMMS SG over  
410 1982-2006 inferred delayed SG trend after mid-1990s over Tibetan Plateau (Yu et al.,  
411 2010). At the North Hemisphere scale, GIMMS SG (1982-2008) showed significant  
412 decadal variation and declining SG shift: advanced 5.2 days over 1982-1999, but only  
413 advanced 0.2 days over 2000-2008 (Jeong et al., 2011). However, the merged  
414 GIMMS (1982-2006) and MODIS (2002-2012) showed SG shift over 2002-2012 ( $-6$   
415  $\text{days decade}^{-1}$ ) is about three times larger than that over 1982-2002 ( $-2 \text{ days decade}^{-1}$ ),  
416 which is interpreted as enhanced SG advancement and its response to temperature  
417 over time (Wang et al., 2016). For the varied timing of SG derived from different  
418 products, Zhang et al. (2017) suggested intersensor calibrations to reduce the  
419 difference between vegetation index products and exclusion of the low quality  
420 phonology timing.

421 These SG shift uncertainties after 2000 are more likely to be explained by the  
422 differences in the NDVI products that implied the opposite SG trend, anomalies north



of 50°N and biome-scale SG-temperature sensitivities. The spectrum range difference of MODIS and AVHRR sensor channels is a main contribute to the NDVI differences. MODIS NDVI is derived from bands 1(620-670nm) and 2 (841-876nm) of the MODIS on board NASA's Terra satellite whereas GIMMS NDVI is derived from bands 1(580-680nm) and 2 (725-1100nm) of AVHRR. The large GIMMS SG anomaly transition around 2000 may be associated with the sensor transition from AVHRR/2 to AVHRR/3, although among-instrument AVHRR calibration were conducted with NDVI data derived from Sea-Viewing Wide Field-of-view Sensor (SeaWiFS) (Pinzon et al., 2014). The calibration with SeaWiFS is considered as an improvement of GIMMS NDVI in the very northern latitudes (Marshall et al, 2016). Even so, the data issues associated with sensor transition, such as (1) satellite signal degradation through lifetime, (2) band design, (3) effect of maximum value composite (MVC) and (4) replacement of satellites in NOAA series, potentially influence the interpretation of the SG trend and its sensitivity to climate drivers.

## 5. Conclusions

We compare the MODIS and GIMMS NDVI inferred time of spring greenup and its response to preseason climate over 2001-2013. We infer a spring greenup delay using GIMMS NDVI in both North America (0.80 days yr<sup>-1</sup>) and Eurasia (0.22 days yr<sup>-1</sup>), whereas, using MODIS NDVI, we infer no significant spring greenup shift in North American and an advanced SG trend of 0.78 days yr<sup>-1</sup> in Eurasia. The differences in MODIS and GIMMS inferred spring greenup trend are mainly in northern high latitude (>50°N). The differences are implied by opposite anomalies in the time of spring greenup in North America and a large GIMMS inferred spring greenup transition around 2000 that maybe explained by data issues associated with the sensor transition from AVHRR/2 to AVHRR/3, including (1) satellite signal



448 degradation through lifetime, (2) band design, (3) effect of maximum value  
449 composite (MVC) and (4) replacement of satellites in NOAA series. Temperature is  
450 the primary climate driver of the time of spring greenup for both MODIS and GIMMS,  
451 although MODIS inferred both a stronger sensitivity and correlation between SG and  
452 temperature. The opposing trends of SG as inferred using MODIS and GIMMS  
453 resulted in differing SG to temperature sensitivity across biomes ( $-3.6 \pm 0.7$  days  $^{\circ}\text{C}^{-1}$   
454 for MODIS and  $2.2 \pm 0.8$  days  $^{\circ}\text{C}^{-1}$  for GIMMS). Using GIMMS, we inferred that the  
455 sensitivity of greenup to temperature, which increases over time for Arctic and boreal  
456 biomes, cannot be well explained by the mechanisms regulating the sensitivity of SG  
457 under a warming climate. This result requires further investigation. Our results  
458 suggest the importance of snow-vegetation interactions in high latitude vegetation  
459 monitoring and inter-validation of multiple datasets to better assess vegetation  
460 dynamics.

461



462    **Acknowledgements**

463    This study is funded by the Strategic Priority Research Program of the Chinese  
464    Academy of Sciences, CASEarth (XDA19070203), grants from CAS Pioneer  
465    Hundred Talents Program and Natural Science Foundation of China (NSFC  
466    #41590853). We acknowledge support from the U.S. Department of Energy, Office of  
467    Science, Biological and Environmental Research, Regional and Global Climate  
468    Modeling Program through the RUBISCO Scientific Focus Area under contract  
469    DE-AC02-05CH11231 to Lawrence Berkeley National Laboratory.

470

471

472

473    **The authors declare no conflicts of interest.**

474

475    **Supplements**

476    **Figure S1**

477    **Figure S2**

478    **Figure S3**

479    **Table S1**



## 480 Reference

- 481 Beck, H. E., T. R. McVicar, A. I. J. M. van Dijk, J. Schellekens, P. A. M. de Jeu,  
482 L. A. Bruijnzeel (2011). Global evaluation of four AVHRR-NDVI data sets:  
483 intercomparison and assessment against Landsat imagery. *Remote Sensing of*  
484 *Environment*, 115, 2547-2563.
- 485 Brown, M. E., J. E. Pinzón, K. Didan, J. T. Morisette, C. J. Tucker (2006).  
486 Evaluation of the consistency of long-term NDVI time series derived from AVHRR,  
487 SPT-Vegetation, SeaWiFS, MODIS, and LandSAT ETM+Sensors. *IEEE*  
488 *Transactions on Geosciences and Remote Sensing*, 44, 1787-1793.  
489 DOI:10.1109/TGRS.2005.860205
- 490 Caffarra, A., A. Donnelly, I. Chuine, M. B. Jones (2011). Modelling the timing  
491 of *Betula pubescens* budburst. I. Temperature and photoperiod: A conceptual model.  
492 *Climate Research*, 46, 147-157.
- 493 Channan, S., K. Collins, and W. R. Emanuel (2014). Global mosaics of the  
494 standard MODIS land cover type data. University of Maryland and the Pacific  
495 Northwest National Laboratory, College Park, Maryland, USA.
- 496 Chen, X., S. Liang, Y. Cao, T. He, D. Wang (2015). Observed contrast changes  
497 in snow cover phenology in northern middle and high latitudes from 2001-2014.  
498 *Scientific Report*, 5, 16820, DOI: 10.1038/srep16820.
- 499 Chmielewski, F. M., & Götz, K.-P. (2016). Performance of models for the  
500 beginning of sweet cherry blossom under current and changed climate conditions.  
501 *Agricultural and Forest Meteorology*, 218–219, 85–91.
- 502 Cong, N., T. Wang, H. Nan, Y. Ma, X. Wang, R. B. Myneni, S. Piao (2013).  
503 Changes in satellite-derived spring vegetation green-up date and its linkage to climate  
504 in China from 1982 to 2010: a multi-method analysis. *Global Change Biology*, 19,  
505 881-891, doi:10.1111/gcb.12077.
- 506 De Beurs, K. M. and G. M. Henebry (2005) Land surface phenology and  
507 temperature variation in the international geosphere-biosphere program high-latitude  
508 transects. *Global Change Biology*, 11, 779-790. Doi: 10.1111/j.1365-  
509 2486.2005.00949.x
- 510 Ding, M., L. Li, Y. Nie, Q. Chen, Y. Zhang (2016) Spatio-temporal variation of  
511 spring phenology in Tibetan Plateau and its linkage to climate change from 1982 to  
512 2012. *Journal of Mountain Science*, 13, 83-94.
- 513 Durpaire, J. P., T. Gentet, T. Phulpin, and M. Arnaud (1995). “Spot-4  
514 Vegetation Instrument: Vegetation Monitoring on a Global Scale.” *Acta Astronautica*,  
515 35, 453-459.
- 516 Fensholt, R. and I. Sandholt (2005). Evaluation of the MODIS and NOAA  
517 AVHRR vegetation indices with in situ measurements in a semi-arid environment.  
518 *International Journal of Remote Sensing*, 26, 2561-2594.
- 519 Fensholt, R., T.T. Nielsen, S. Stisen (2006). Evaluation of AVHRR PAL and  
520 GIMMS 10-day composite NDVI time series products using SPOT-4 vegetation data  
521 for the African continent. *International Journal of Remote Sensing*, 27, 13, 2719-2733,  
522 DOI:10.1080/01431160600567761



- 523 Fensholt, R., K. Rasmussen, T. T. Nielsen, C. Mbow (2009). Evaluation of earth  
524 observation based long term vegetation trends-intercomparing NDVI time series trend  
525 analysis consistency of Sahel from AVHRR GIMMS, Terra MODIS and SPOT VGT  
526 data. *Remote Sensing of Environment*, 113, 1886-1898.
- 527 Fensholt, R. and S. R. Proud (2012). Evaluation of Earth Observation based  
528 global long term vegetation trends- Comparing GIMMS and MODIS global NDVI  
529 time series. *Remote Sensing of Environment*, 119, 131-147.
- 530 Friedl, M.A., D. Sulla-Menashe, B. Tan, A. Schneider, N. Ramankutty, A.  
531 Sibley and X. Huang (2010). MODIS Collection 5 global land cover: Algorithm  
532 refinements and characterization of new datasets, 2001-2012, Collection 5.1 IGBP  
533 Land Cover, Boston University, Boston, MA, USA.
- 534 Gong, Z., K. Kawamura, N. Ishikawa, M. Goto, T. Wulan, D. Alateng, T. Yin,  
535 Y. Ito (2015) MODIS normalized difference vegetation index (NDVI) and vegetation  
536 phenology dynamics in the Inner Mongolia grassland. *Solid Earth*, 6, 1185-1194. Doi:  
537 10.5194/se-6-1185-2015.
- 538 Høgda, K. A., H. Tømmervik, S. R. Karlsen (2013) Trends in the start of the  
539 growing season in Fennoscandia 1982-2011. *Remote Sensing*, 5, 4304-4318. Doi:  
540 10.3390/rs5094304.
- 541 Jeong, S.J., C. H. Ho, J. H. Jeong (2009) Increase in vegetation greenness and  
542 decrease in spring time warming over East Asia. *Geophysical Research Letters*, 36,  
543 L0270, doi: DOI: 10.1029/2008GL036583
- 544 Jeong, S.-J., C.-H. Ho, H.-J. Gim, M. E. Brown (2011). Phenology shifts at start  
545 vs. end of growing season in temperate vegetation over the Northern Hemisphere for  
546 the period 1982-2008. *Global Change Biology*, 17, 2385-2399, doi: 10.1111/j.1365-  
547 2486.2011.02397.x
- 548 Julien, Y., J. A. Sobrino (2009) Global land surface phenology trends from  
549 GIMMS database. *International Journal of Remote Sensing*, 30, 3495–3513.
- 550 Karlsen, S.R., K. A. Høgda, F. E. Wielgolaski, A. Tolvanen, H. Tømmervik, J.  
551 Poikolainen, E. Kubin (2009) Growing-season trends in Fennoscandia 1982–2006,  
552 determined from satellite and phenology data. *Climate Research*, 39, 275–286.
- 553 Keenan, T. F., B. Darby, E. Felts, O. Sonnentag, M. A. Friedl, K. Hufkens, J.  
554 O’Keefe, S. Klosterman, J. W. Munger, M. Toomey, A. D. Richardson (2014)  
555 Tracking forest phenology and seasonal physiology using digital repeat photography:  
556 a critical assessment. *Ecological Applications*, 24, 1478-1489. Doi:10.1890/13-0652.1
- 557 Kern, A., H. Marjanović, Z. Barcza. (2016). Evaluation of the quality of  
558 NDVI3g Dataset against collection 6 MODIS NDVI in central Europe between 2000  
559 and 2013. *Remote Sensing*, 8, 955; doi:10.3390/rs8110955.
- 560 Lee, R., F. Yu, K. P. Price, J. Ellis, P. Shi (2002) Evaluating vegetation  
561 phenological patterns in Inner Mongolia using NDVI time-series analysis.  
562 *International Journal of Remote Sensing*, 23, 2505-2512.  
563 Doi:10.1080/01431160110106087
- 564 Marshall, M., E. Okuto, Y. Kang, E. Opiyo, M. Ahmed. (2016). Global  
565 assessment of vegetation index and Phenology Lab (VIP) and Global Inventory  
566 Modeling and Mapping Studies (GIMMS) version 3 products. *Biogeosciences*, 13,  
567 625-639.



- 568 Myneni, R. B., C. D. Keeling, C. J. Tucker, G. Asrar, R. R. Nemani (1997).  
569 Increased plant growth in the northern high latitudes from 1981 to 1991. *Nature*, 386,  
570 698-702.
- 571 Oberbauer, S.F., S. C. Elmendorf, T. G. Troxler et al. (2013). Phenological  
572 response of tundra plants to background climate variation tested using the  
573 International Tundra Experiment. *Philosophical Transactions of the Royal Society B:*  
574 *Biological Sciences*, 368, 20120481. DOI: 10.1098/rstb.2012.0481
- 575 Piao, S. L., J. Y. Fang, L. M. Zhou, P. Ciais, B. Zhu(2006) Variations in  
576 satellite-derived phenology in China's temperate vegetation. *Global Change Biology*,  
577 12, 672-685.
- 578 Piao, S., H. Nan, C. Huntingford, P. Ciais, P. Friedlingstein, S. Sitch, S. Peng, A.  
579 Ahlström, J. G. Canadell, N. Cong, S. Levis, P. E. Levy, L. Liu, M. R. Lomas, J.  
580 Mao, R. B. Myneni, P. Peylin, B. Poulter, X. Shi, G. Yin, N. Viory, T. Wang, X.  
581 Wang, S. Zaehle, N. Zeng, Z. Zeng, A. Chen (2014). Evidence for a weakening  
582 relationship between interannual temperature variability and northern vegetation  
583 activity. *Nature Communications*, doi:10.1038/ncomms6018.
- 584 Pinzon, J. E., C. J. Tucker (2014). A non-stationary 1981-2012 AVHRR  
585 NDVI3g time series. *Remote Sensing*, 6, 6929-6960. doi:10.3390/rs6086929
- 586 Prevéy, J., M. Vellend, N. Rüger, R. D. Hollister, A. D. Bjorkman, I. H. Myers-  
587 Smith, S. C. Elmendorf, K. Clark, E. J. Cooper, B. Elberling, A. M. Fosaa, G. H. R.  
588 Henry, T. T. Høye, I. S. Jónsdóttir, K. Klanderud, E. Lévesque, M. Mauritz, U. Molau,  
589 S. M. Natali, S. F. Oberbauer, Z. A. Panchen, E. Post, S. B. Rumpf, N. M. Schmidt, E.  
590 A. G. Schuur, P. R. Semenchuk, T. Troxler, J. M. Welker, C. Rixen (2017). Greater  
591 temperature sensitivity of plant phenology at colder sites: implications for  
592 convergence across northern latitudes. *Global Change Biology*, 23, 2660-2671, DOI:  
593 10.1111/gcb.13619.
- 594 Semenchuk, P. R., M. A. K. Gillespie, S. B. Rumpf, N. Baggesen, B. Elberling,  
595 E. J. Cooper (2016). High Arctic plant phenology is determined by snowmelt patterns  
596 but duration of phenological periods is fixed: an example of periodicity.  
597 *Environmental Research Letters*, 125006. DOI: 10.1088/1748-9326/11/12/125006.
- 598 Shen M., Y. Tang Y, J. Chen, X. Yang, C. Wang, X. Cui, Y. Yang, L. Han, L.  
599 Li, J. Du, G. Zhang, N. C (2014). Earlier-Season Vegetation Has Greater Temperature  
600 Sensitivity of Spring Phenology in Northern Hemisphere. *PLoS ONE* 9(2): e88178.  
601 DOI:10.1371/journal.pone.0088178
- 602 Stöckli, R. and P. L. Vidale (2004) European plant phenology and climate as  
603 seen in a 20-year AVHRR land-surface parameter dataset. *International Journal of*  
604 *Remote Sensing*, 25, 3303-3330. Doi: 10.1080/01431160310001618149
- 605 Tang, G., J. A. Arnone III, P. S. J. Verburg, R. L. Jasoni, L. Sun (2015) Trends  
606 and climatic sensitivities of vegetation phenology in semiarid and arid ecosystems in  
607 the US Great Basin during 1982-2011. *Biogeosciences*, 12, 6985-6997.  
608 Doi:10.5194/bg-12-6985-2015
- 609 Tong, A. and Y. He (2013). Comparative analysis of SPOT, Landsat, MODIS  
610 and AVHRR normalized difference vegetation index data on the estimation of leaf  
611 area index in a mixed grassland ecosystem. *Journal of Applied Remote Sensing*, 7,  
612 073599-1-15.



- 613 Tucker, C. J., D. A. Slayback, J. E. Pinzon, S. O. Los, R. B. Myneni, M. G.  
614 Taylor (2001) Higher northern latitude NDVI and growing season trends from 1982 to  
615 1999. *International Journal of Biometeorology*, 45, 184-190. Doi: 10.1007/s00484-  
616 001-0109-9.
- 617 Wang, S., B. Yang, Q. Yang, L. Lu, X. Wang, Y. Peng (2016). Temporal trends  
618 and spatial variability of vegetation phenology over the Northern Hemisphere during  
619 1982-2012. *PLoS ONE*, 11, e0157134. doi:10.1371/journal.pone.0157134
- 620 Wu, X., H. Liu, X. Li, S. Piao, P. Ciais, W. Guo, Y. Yin, B. Poulter, C. Peng, N.  
621 Viory, N. Vuichard, P. Wang, Y. Huang (2017). Higher temperature variability  
622 reduces temperature sensitivity of vegetation growth in Northern Hemisphere.  
623 *Geophysical Research Letters*, Doi: 10.1002/2017GL073285
- 624 Xu, X., W.J. Riley, C. D. Koven, G. Jia (2018). Observed and simulated  
625 sensitivities of spring greenup to pre-season climate in northern temperate and boreal  
626 regions. *Journal of Geophysical Research: Biogeoscience*, 123: 60-78. doi:  
627 10.1002/2017jg004117
- 628 Yang, B., M. He, V. Shishov, I. Tychkov, E. Vaganov, S. Rossi, F. C.  
629 Ljungqvist, A. Bräuning, J. Griesinger (2017). New perspective on spring vegetation  
630 phenology and global climate change based on Tibetan Plateau tree-ring data.  
631 *Proceedings of the National Academy of Sciences of the United States of America*,  
632 114, 6966-6971.
- 633 Yu, H., E. Luedeling, J. Xu (2010). Winter and spring warming result in  
634 delayed spring phenology on the Tibetan Plateau, *Proceedings of the National*  
635 *Academy of Sciences of the United States of America*, 107, 22151-22156.
- 636 Zeng, H., G. Jia, H. Epstein (2011) Recent Changes in Phenology over the  
637 northern high latitudes detected from multi-satellite data. *Environmental Research*  
638 *Letters*, 045508. Doi: 10.1088/1748-9326/6/045508
- 639 Zeng, H., G. Jia, B. C. Forbes (2013). Shifts in Arctic phenology in response to  
640 climate and anthropogenic factors as detected from multiple satellite time series.  
641 *Environmental Research Letters*, 8, 035036. Doi:10.1088/1748-9326/8/3/035036.
- 642 Zeng, H. and G. Jia (2013). Impacts of snow cover on vegetation phenology in  
643 the Arctic from satellite data. *Advances in Atmospheric Sciences*, 30, 1421-1432.
- 644 Zhang, X., Friedl, M.A., Schaaf, C.B., Strahler, A.H., Hodges, J.C.F., Gao, F.,  
645 Reed, B.C., Huete, A. (2003). Monitoring vegetation phenology using MODIS.  
646 *Remote Sensing of Environment*, 84, 471-475.
- 647 Zhang, G., Y. Zhang, J. Dong, X. Xiao (2013). Green-up dates in the Tibetan  
648 Plateau have continuously advanced from 1982-2011. *Proceedings of the National*  
649 *Academy of Sciences of the United States of America*, 110, 4309-4314.
- 650 Zhang, X., L. Liu, D. Yan (2017). Comparisons of global land surface  
651 seasonality and phenology derived from AVHRR, MODIS, and VIIRS data. *Journal*  
652 *of Geophysical Research: Biogeosciences*, 122, 1506-1525.
- 653 Zhou, J., L. Jia, M. Menenti (2015). Reconstruction of global MODIS NDVI  
654 time series: Performance of Harmonic Analysis of Time Series (HANTS). *Remote*  
655 *Sensing of Environment*, 163, 217-228. DOI: 10.1016/j.rse.2015.03.018



**Figure Captions:**

Figure 1. The GIMMS (a) and MODIS (b) inferred mean Julian date of spring greenup ( $\bar{D}_{SG}$ , day of year) over 2001-2013 and GIMMS (c) and MODIS (d) inferred trend of spring greenup date ( $D_{SG}$ ) over 2001-2013(days yr<sup>-1</sup>).

Figure 2 Anomalies of spring greenup date for mid-latitude (30-50°N, a, c, e) and high latitude (>50°N, b, d, f) in relative to mean  $D_{SG}$  over 2001-2013 for GIMMS and MODIS.

Figure 3 Mean pre-season length of temperature control corresponding to GIMMS spring greenup ( $\bar{L}_{PT}^G$ , days) and MODIS spring greenup ( $\bar{L}_{PT}^M$ , days) and mean pre-season length of precipitation control corresponding to GIMMS spring greenup ( $\bar{L}_{PP}^G$ , days) and MODIS greenup ( $\bar{L}_{PP}^M$ , days).

Figure 4 Spring greenup sensitivity to pre-season temperature (days °C<sup>-1</sup>) for GIMMS (a) and MODIS (b) and spring greenup sensitivity to pre-season precipitation (days %<sup>-1</sup> of precipitation increases) for GIMMS (c) and MODIS (d).

Figure 5 The comparison of inter-biome SG sensitivity to pre-season temperature for IGBP land cover types for GIMMS over 1982-2005 and 2001-2013 and MODIS over 2001-2013. We used the IGBP land cover classification for 9 biomes in 2012: Evergreen Needleleaf Forest (ENF), Deciduous Needleleaf Forest (DNF), Deciduous Broadleaf forest (DBF), Mixed Forest (MF), Open Shrublands (OS), Woody Savannas (WS), Grassland (GL), Permanent Wetland (PW), and Cropland (CP). We distinguish the Arctic grassland to the north of 60°N (GLN), from temperate grassland in the south (GLS) due to their expected differences in climate and controls on phenology.



Table 1 The spring greenup shift (days per decade) as inferred from Normalized Difference Vegetation Index (NDVI) from satellite data

NDVI Data	Period	Region	Shift (days decade <sup>-1</sup> )	Reference
PAL	1981-1991	>=40N	-8	Myneni et al., 1997
GIMMS	1981-1999	Eurasia	-3.3	Zhou et al., 2001
GIMMS	1981-1999	N. America	-4.4	Zhou et al., 2001
AVHRR	1982-1991	45-75	-6.2	Tucker et al., 2001
AVHRR	1992-1999	45-75	-2.4	Tucker et al., 2001
AVHRR	1982-1990	Inner Mongolia	0	Lee et al., 2002
PAL	1982-2001	Europe	-5.4	Stockli and Vidale, 2004
PAL	1985-1999	N. America	-6.6	de Beurs and Henebry, 2005
PAL	1985-2000	Eurasia	-4.5	de Beurs and Henebry, 2005
GIMMS	1982-1999	Temperate China	-7.9	Piao et al., 2006
PAL	1982-1999	East Asia	-7	Jeong et al., 2009
GIMMS	1982-2003	Global	-3.8	Julien & Sobrino, 2009
GIMMS	1982-2006	Fennoscandia	-2.7	Karlsen et al., 2009
GIMMS	1982-1999	N. Hemisphere	-2.9	Jeong et al., 2011
GIMMS	2002-2008	N. Hemisphere	-0.3	Jeong et al., 2011
MODIS	2000-2010	>60N, Arctic	-4.7	Zeng et al., 2011
MODIS	2000-2010	>60N, N. America	-11.5	Zeng et al., 2011
MODIS	2000-2010	>60N, Eurasia	-2.7	Zeng et al., 2011
GIMMS	1982-2008	>60N, Arctic	-0.5	Zeng et al., 2011
GIMMS	1982-2008	>60N, N. America	-0.8	Zeng et al., 2011
GIMMS	1982-2008	>60N, Eurasia	-0.3	Zeng et al., 2011
GIMMS SPOT-VGT	1982-2011	Tibetan Plateau	-10.4	Zhang et al., 2013
GIMMS	1982-2011	Fennoscandia	-11.8	Høgda et al., 2013
MODIS	2001-2012	U.S.	-4.8	Keenan et al., 2014
MODIS	2002-2014	Inner Mongolia	-4.5	Gong et al., 2015
GIMMS	1982-2011	U.S. Great Basin	-0.1	Tang et al., 2015
GIMMS	1982-2002	N. Hemisphere	-1.9	Wang et al., 2016
MODIS	2002-2012	N. Hemisphere	-5.9	Wang et al., 2016
GIMMS	1982-2012	Tibetan Plateau	0	Ding et al., 2016

MODIS: Moderate Resolution Imaging Spectroradiometer

AVHRR: Advanced Very High Resolution Radiometer

GIMMS: Global Inventory Modeling and Mapping Studies

PAL: Pathfinder AVHRR Land

GAC: Global area cover

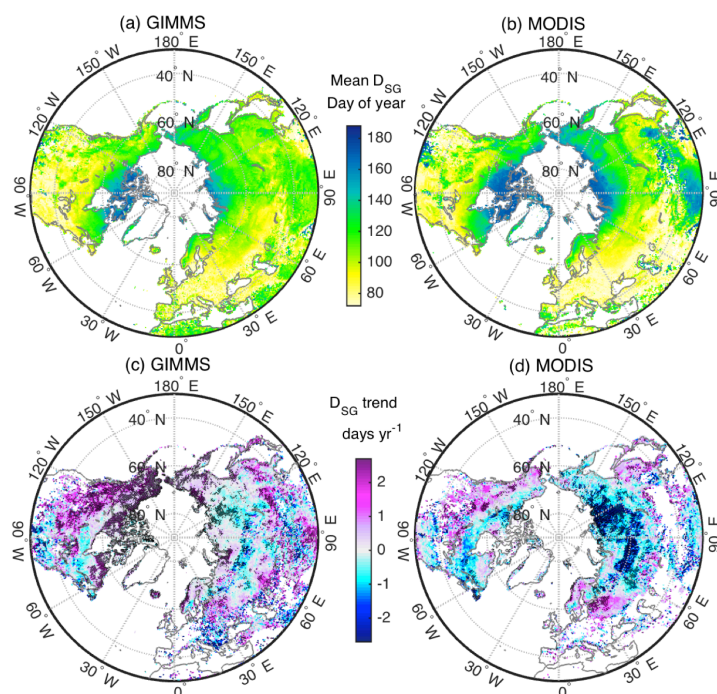


Figure 1. The GIMMS (a) and MODIS (b) inferred mean Julian date of spring greenup ( $\bar{D}_{SG}$ , day of year) over 2001-2013 and GIMMS (c) and MODIS (d) inferred trend of spring greenup date ( $D_{SG}$ ) over 2001-2013 (days yr<sup>-1</sup>).

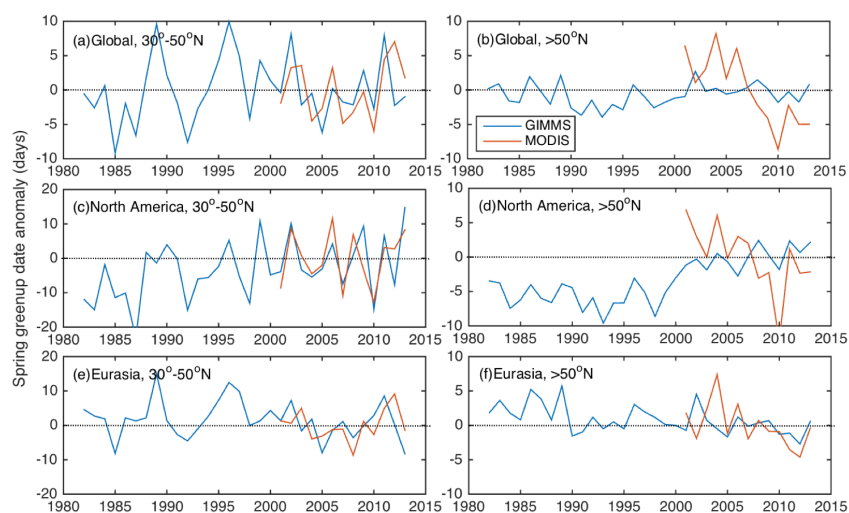


Figure 2 Anomalies of spring greenup date for mid-latitude (30°-50° N, a, c, e) and high latitude (>50° N, b, d, f) in relative to mean  $D_{SG}$  over 2001-2013 for GIMMS and MODIS.

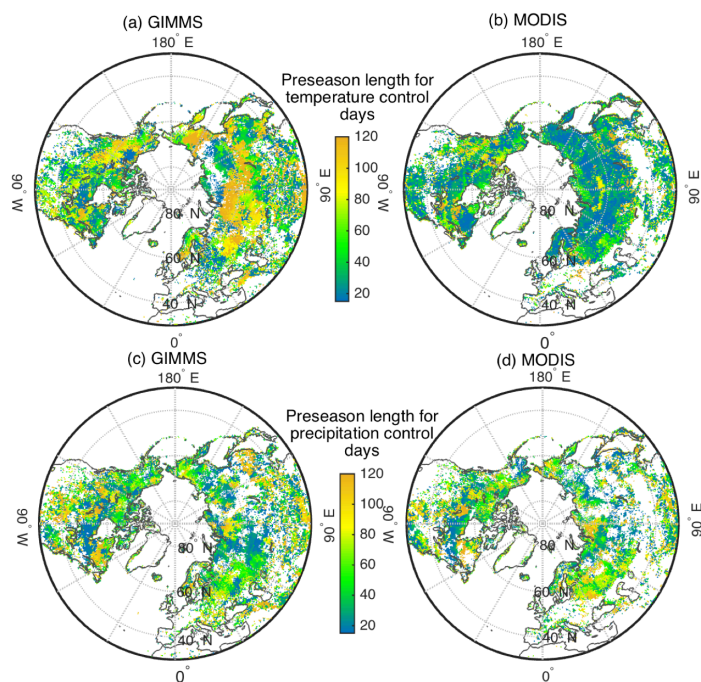


Figure 3 Mean preseason length of temperature control corresponding to GIMMS spring greenup ( $\bar{L}_{pT}^G$ , days) and MODIS spring greenup ( $\bar{L}_{pT}^M$ , days) and mean preseason length of precipitation control corresponding to GIMMS spring greenup ( $\bar{L}_{pP}^G$ , days) and MODIS greenup ( $\bar{L}_{pP}^M$ , days).

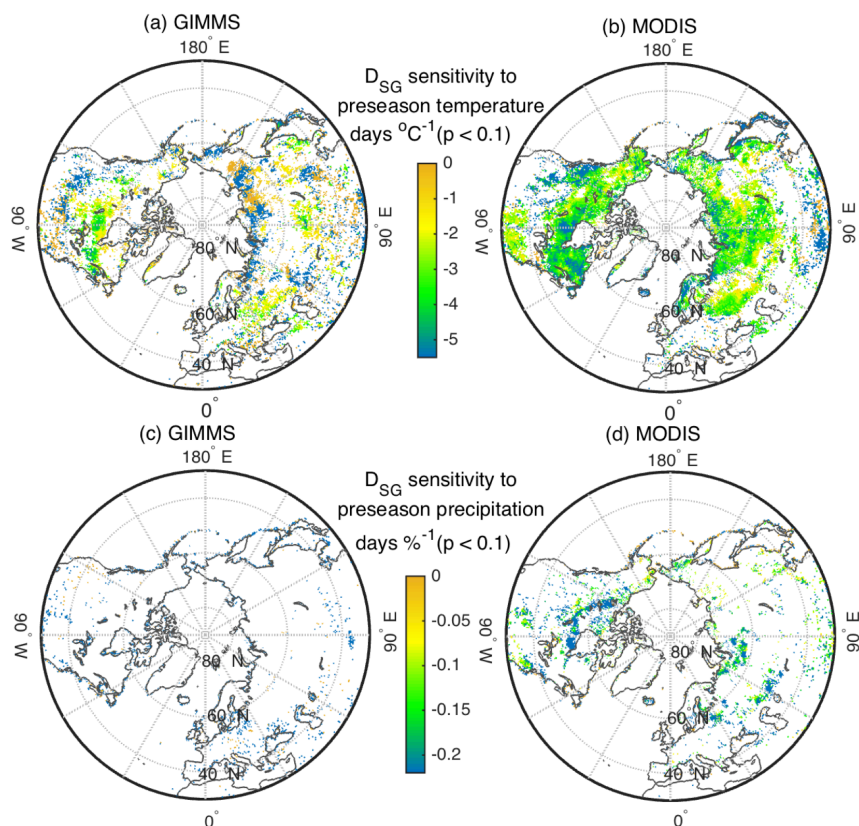


Figure 4 Spring greenup sensitivity to preseason temperature (days  $^{\circ}\text{C}^{-1}$ ) for GIMMS (a) and MODIS (b) and spring greenup sensitivity to preseason precipitation (days  $\%^{-1}$  of precipitation increases) for GIMMS (c) and MODIS (d).

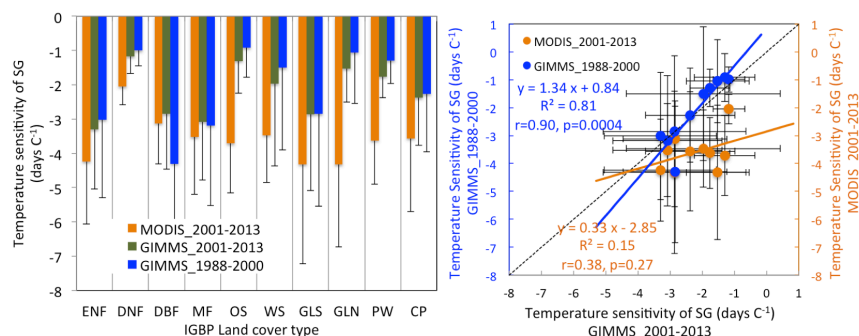


Figure 5 The comparison of inter-biome SG sensitivity to preseason temperature for IGBP land cover types for GIMMS over 1982-2005 and 2001-2013 and MODIS over 2001-2013. We used the IGBP land cover classification for 9 biomes in 2012: Evergreen Needleleaf Forest (ENF), Deciduous Needleleaf Forest (DNF), Deciduous Broadleaf forest (DBF), Mixed Forest (MF), Open Shrublands (OS), Woody Savannas (WS), Grassland (GL), Permanent Wetland (PW), and Cropland (CP). We distinguish the Arctic grassland to the north of 60°N (GLN), from temperate grassland in the south (GLS) due to their expected differences in climate and controls on phenology.